Appl. Phys. A (2016) 122:808
DOI 10.1007/s00339-016-0336-9

Applied Physics A
Materials Science & Processing

CrossMark

Effects of thickness layer on the photoluminescence properties of InAlAs/GaAlAs quantum dots

A. Ben Daly[1] · F. Bernardot[2,3] · T. Barisien[2,3] · E. Galopin[4] · A. Lemaître[4] · M. A. Maaref[1] · C. Testelin[2,3]

Received: 18 May 2016 / Accepted: 2 August 2016 / Published online: 10 August 2016
© Springer-Verlag Berlin Heidelberg 2016

Abstract We investigated the effect of InAlAs layer thickness on exciton-spin relaxation and optical properties of $In_{0.62}Al_{0.38}As/Al_{0.67}Ga_{0.33}As$ QDs. The luminescence properties and carrier dynamics of QDs were studied by the temperature-dependent photoluminescence (PL) and pump-probe measurements. As the total amount of deposited In0.62Al0.38As alloy increased, the central position of the low-energy PL signal decreases, while its full width at half maximum (FWHM) increases. A monotonous redshift of the PL peak was observed with increasing temperature due to the electron–phonon scattering. From the pump-probe measurement, the spin relaxation time decreases with the monolayers at higher temperatures, in agreement with the phonon energy determinate by PL measurements.

1 Introduction

Charge carriers can be confined in more than one dimension, if different semiconductor heterostructures are grown. If the dimension is smaller than the de Broglie wavelength in two directions, the resulting object is called a nanowire. When charge carriers are confined in all three dimensions, the structure is called quantum dot (QD). Semiconductor QDs are of great interest in many device applications such as photodetectors, labels for biological imaging and different types of memories [1–3]. In fact, QDs are given by a series of delta functions and depend just on the number of confined levels. A fundamental understanding of the carrier dynamics in QDs needs to be developed to allow optimisation of the desired properties. The carriers are localised in the area of the dot due to the effectively increased thickness of the layer. By photoluminescence (PL) and pump-probe techniques, it becomes possible to understand how layer thickness affects the confinement of the carriers in the structures and thus their spin relaxation. This work will focus on self-assembled InAlAs QDs, produced by Stranski–Krastanov growth. The InAlAs/GaAlAs QD system with emission in the visible region [4] features a variety of interesting characteristics such as inhomogeneous broadening, arises from the superposition of many transitions in a QD ensemble [5–7], state filling and excited-state emission [8], and Distinctive carrier dynamics and phonon interaction [9]. The uniformity of InAlAs dots depends strongly on growth conditions [10, 11]. The optical studies [12, 13] revealed its excellent relaxation time, which usually gives a long spin relaxation time. Pump-probe is a powerful tool for the investigation of carrier dynamics in semiconductors [13–15]. In this study, we investigated the effect of InAlAs layer thickness on exciton-spin relaxation and optical properties of $In_{0.62}Al_{0.38}As/Al_{0.67}Ga_{0.3}3As$ QDs. The luminescence properties and carrier dynamics of QDs were studied by the temperature-dependent photoluminescence (PL) and pump-probe measurements.

✉ A. Ben Daly
amenibendaly@gmail.com

[1] Laboratoire Matériaux, Molécules et Applications, Institut Préparatoire aux Études Scientifiques et Techniques, Université de Carthage, BP 51, 2070 La Marsa, Tunis, Tunisia

[2] Sorbonne Universités, UPMC Université Paris 06, UMR 7588, Institut des NanoSciences de Paris, 75005 Paris, France

[3] CNRS, UMR 7588, INSP, 75005 Paris, France

[4] Laboratoire de Photonique et Nanostructures, CNRS, UPR 20, Route de Nozay, 91460 Marcoussis, France

2 Experimental

The three samples studied in this work follow a similar growth procedure. The QD sample was prepared by molecular-beam epitaxy and is similar to previously studied samples [16]: the growths of the $In_{0.62}Al_{0.38}As$ QDs were performed on a 100-nm-thick $Ga_{0.67}Al_{0.33}As$ epilayer and were monitored by reflection high-energy electron diffraction (RHEED). The QDs were covered by a $Ga_{0.67}Al_{0.33}As$ epilayer of same composition and same thickness. Figure 1 presents a sketch of the sample structure: it contains a single plane of $In_{0.62}Al_{0.38}As$ QDs.

The growth temperature is around 560 °C for all samples. The growth rate is similar for all samples and is about 0.92 monolayer per second (ML/s). The critical thickness, at which the growth turns from two-dimensional (deposition of $In_{0.62}Al_{0.38}As$ layers) to three-dimensional (appearance of $In_{0.62}Al_{0.38}As$ QDs), is detected on the RHEED pattern. It is measured during the growth process at about 3.7 monolayers.

During the PL measurement, the sample was in a variable-temperature He-cryostat (4–150 K), on a cold finger. In the PL studies, the sample was excited by laser diode at 405 nm and focused on the sample in a 100-μm-diameter spot. The resulting PL was dispersed by a monochromator and detected by a silicon avalanche photodiode.

For the pump-probe measurements, a femtosecond titanium–sapphire laser was used, possessing a 76-MHz repetition rate. The main laser beam falls on a beam splitter to create the pump and probe beams; their powers (50 and 2 mW, respectively) are tuned with half-wave plates and polarisers. Both beams impinge the sample quasi-normally (i.e. along the growth axis [001]), in superimposed spots of diameter around 100 μm. After reflection on the sample, the pump beam is stopped, and the probe one enters a balanced optical bridge, which measures its polarisation rotation created by the pumped sample. The time delay between the probe pulses and the pump ones is controlled by a retardation line. The edges of the sample, along the [110] and [1−10] azimuths which were used as indication along these directions, are settled horizontally and vertically in the experiment.

The pump polarisation is chosen horizontal or vertical, whereas the probe one is always 45° slanted from the [110] and [1−10] directions. Using the optical bridge, this orientation of the probe polarisation allows the extraction of an electronic signal proportional to the difference in the populations of the X and Y excitons, which are linearly polarised along [110] and [1−10] (these X and Y states are spin states with respect to an in-plane quantification axis [17]). The pump beam is modulated at 50 kHz with an acousto-optic modulator, and the modulation on the probe is made by a mechanical chopper (at 250 Hz), and the signal is detected with a double lock-in demodulation.

The sample was set on a cold finger in a helium-gas-flow cryostat; its temperature can be regulated between 6 and 100 K.

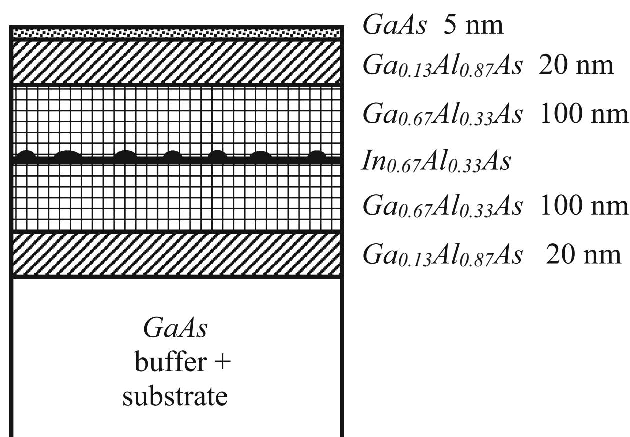

Fig. 1 Structure of the studied samples, consisting of a single layer of $In_{0.67}Al_{0.33}As$ QDs

3 Results and discussion

The PL spectra of the three samples obtained at low temperature are shown in Fig. 2. Curves 2(a), 2(b) and 2(c) concern the 6.4, 5.5 and 4.2 ML samples, respectively.

The narrow line systematically measured at 1.94–2.00 eV, with full width at half maximum (FWHM) 12–15 meV, is attributed to the PL of the $Ga_{0.67}Al_{0.33}As$ symmetric barrier. The spectrally broad PL signal observed at lower energies comes from fundamental optical transitions within the $In_{0.62}Al_{0.38}As$ QDs. In curve 2(a), such a

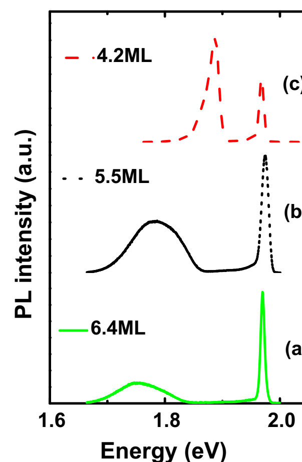

Fig. 2 Low-temperature PL spectra of the studied samples **a** 6.4 ML; **b** 5.5 ML and **c** 4.2 ML. The narrow line near 2 eV is due to the $Ga_{0.67}Al_{0.33}As$ barrier; the low-energy PL signal, spectrally broad, arises from the $In_{0.67}Al_{0.33}As$ QDs

PL signal is centred at 1.747 eV and possesses a FWHM of 91 meV. In curve 2(b), the maximum of the low-energy PL signal is located at 1.786 eV, and the corresponding FWHM is 99 meV. In curve 3(c), this PL maximum is observed at 1.886 eV, and the FWHM is 22.5 meV. The low-energy PL signal shifts towards lower energies and broadens as the amount of $In_{0.62}Al_{0.38}As$ deposition is increased.

We first qualitatively interpreted the low-energy signal in the PL spectra shown in Fig. 2, following two guidelines: (1) in samples in which this structure is narrow (typically 22.5 nm), we suspect that the optical emission comes from wetting layers (WL), possibly with roughness and/or with QDs of so small sizes that they confine no photo-created carriers; (2) in samples in which this structure is broad 5.5 and 6.4 ML, the optical emission is probably due to confining QDs, the size distribution of which explains the inhomogeneous spectral broadness. Specifically, for the three $x = 0.38$ samples (see Fig. 2), the plots in Fig. 3 appear to confirm a transition from regime (1) to regime (2): as the total amount of deposited $In_{0.62}Al_{0.38}As$ alloy is increased from 4.2 to 5.5 and 6.4 ML, the central position of the low-energy PL signal suddenly decreases in energy (from 1.89 to 1.77 eV), while its FWHM abruptly increases (from 20 to 100 meV). Another feature of QDs must be taken into account: As of today, no set of self-assembled QDs consists of identically shaped and sized QDs. Due to the nature of the growth process, they exhibit a stochastic distribution of sizes, which in turn changes their confinements and spectral parameters [18]. This can be measured as a broadening of the collective spectrum, referred to as ‘inhomogeneous broadening’ (see Fig. 2), as compared to the natural linewidth of a single QD (called ‘homogeneous broadening’).

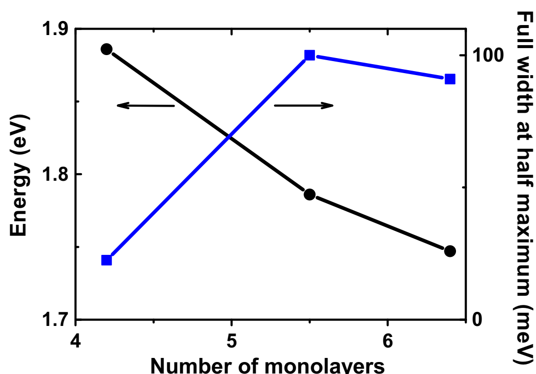

Fig. 3 Central energy E (*full circles*, *left vertical axis*) and FWHM (*full squares*, *right axis*) of the low-energy PL signal shown by the three $x = 0.38$ samples (see Fig. 2); the *horizontal axis* represents the total amount of deposited $In_{0.67}Al_{0.33}As$. The optical emission appears to turn from a one due to a WL to another arising from inhomogeneous QDs

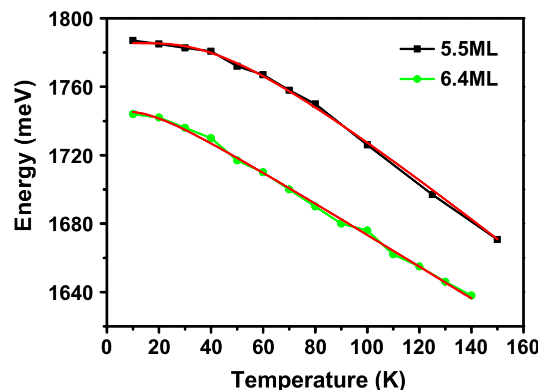

Fig. 4 GS PL peak energies measured at various temperatures. *Symbols* are the experimental data, and the continuous *red line* are calculated from Bose–Einstein law (see text)

Figure 4 shows the ground state PL peak energies measured at various temperature for 5.5 and 6.4 ML. As schematically indicated in Fig. 4, a monotonous redshift of the PL peak position was observed with increasing temperature [19], photogenerated carriers transfer and relax into energetically low-lying states, giving rise to the fast redshift of the exciton energy. The temperature dependence can be well reproduced by the following Bose–Einstein [20] equation:

$$E_g(T) = E_g(0) - \frac{\lambda}{\exp\left(\frac{\hbar\omega_{ph}}{k_B T}\right) - 1}$$

where $E_g(0)$ is the band gap at 0 K, λ is the constant of the electron–phonon coupling strength, and finally $\hbar\omega_{ph}$ refers to the phonon energy. The used values for the fits of Fig. 4 are $\hbar\omega_{ph} = 9.5 \pm 0.8$ and $\hbar\omega_{ph} = 4.7 \pm 0.7$ meV, respectively, for 5.5 and 6.4 ML. One can note that the phonon energy is very close to the transverse acoustic mode TA (L) in $In_{0.62}Al_{0.38}As$ estimated at 5.6 meV, from an interpolation between the InAs and AlAs TA (L) energies equal to 4.7 and 7 meV, respectively [21, 22]. The role of the transverse acoustic modes in the temperature dependence of the band gap energy has already been evidenced in GaAs bulk and InGaAs QDs [23, 24]. The emission energy of the InAlAs layer is found to decrease with increasing layer thickness, resulting from the enhanced carrier relaxation process related to the size distribution of QDs [25].

In pump-probe experiments, we have studied the exciton-spin relaxation of samples B (5.5 ML) and C (6.4 ML). The mode-locking of this laser can occur in the wavelength range from 700 to 1000 nm; this explains that we could not have studied the sample A (4.2 ML), with exciton ground states emitting at wavelengths shorter than 700 nm (see Fig. 2).

For several temperatures between 10 and 80 K, Fig. 5 shows the pump-probe signals measured on sample B

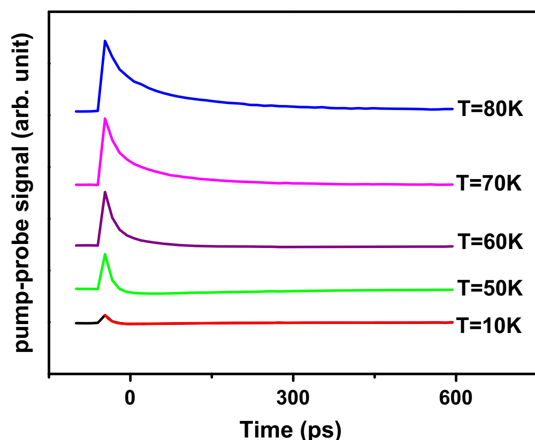

Fig. 5 Pump-probe signals measured on sample B (5.5 ML), for several temperatures between 10 and 80 K. The pump polarisation is horizontal. The continuous line on the 10 K curve is a biexponential fit of its decay

(5.5 ML), as a function of the pump-probe delay; the pump polarisation is horizontal. The laser wavelength is tuned to the (temperature-dependent) PL maximum of the sample. A typical pump-probe signal exhibits a fast-decay component, followed by a slow decay to zero. The fast-decay part of the signals arises from the GaAs substrate, whose band gap wavelength is longer than the laser one: as the laser photon energy is tuned below the lowest one of the confined exciton fundamental states, the fast decay is still present in the pump-probe signal, while the slow decay vanishes. So we attributed the slow-decay component observed on the pump-probe signal to the spin relaxation of the excitons confined in the $In_{0.67}Al_{0.33}As$ QDs. This slow decay is fitted to a mono-exponential function; we extract a characteristic relaxation time τ_{ps} for each sample temperature, and for each horizontal or vertical polarisation of the pump beam. The analysis of the pump-probe signals recorded on samples B (5.5 ML) and C (6.4 ML) is presented in Fig. 6, where the experimental data are plotted (green continuous line) for samples B (5.5 ML) (Fig. 6a) and C (6.4 ML) (Fig. 6b). The spin relaxation times τ_{ps} [H] and τ_{ps} [V], corresponding, respectively, to horizontal and vertical pump beam polarisations, are plotted as functions of temperature. For sample B (5.5 ML), the pump-probe signals could have been exploited from 10 to 80 K, and 6 to 100 K for sample C (6.4 ML). In Fig. 6, the measured τ_{ps} [H] (τ_{ps} [V]) values are represented by black squares (circles): we observe that the measured spin relaxation time is essentially independent of the pump polarisation, and we then retain a mean behaviour τ_{ps} of this spin relaxation time, shown in the figure by the continuous line. For sample C (6.4 ML), τ_{ps} is around 250–400 ps for temperatures below 70 K, and abruptly falls for higher temperatures. For sample B (5.5 ML), τ_{ps} is

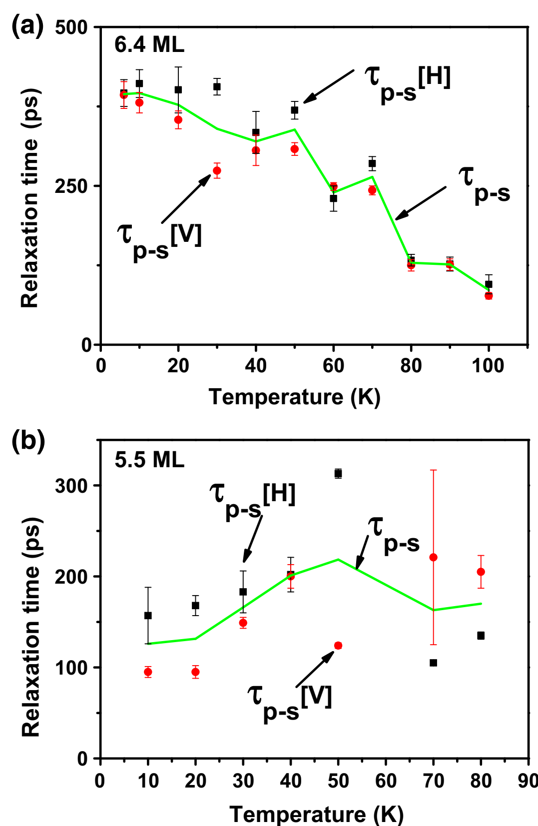

Fig. 6 Pump-probe τ_{ps} [H], *black squares* (respectively, τ_{ps} [V], *red circles*), characteristic slow-decay times measured on samples **a** B (5.5 ML) and **b** C (6.4 ML), with a pump beam horizontally (respectively, vertically) polarised. The line shows the mean τ_{ps} behaviour with temperature

constant about 126 ps, increases above 30 K and decreases for higher temperatures.

The spin relaxation time increases with the monolayers at low temperature can be explained by the thermal activation of the nonradiative process. When the temperature increases, the thermal activation of carriers becomes dominant and the spin relaxation decreases with the monolayers due to the electron–phonon scattering, which decreases from 9.5 to 4.7 meV, respectively, for 5.5 and 6.4 ML.

4 Conclusions

We have investigated the PL and pump-probe properties of a visible emitting InAlAs/GaAlAs QD sample grown on a GaAs substrate. A sudden decrease in the PL energy emission with increasing InAlAs thickness indicates that the optical emission comes from WL to QDs, while the FWHM abruptly increases due the efficient relaxation process. A strong decrease in the relaxation time with

increasing monolayers has been observed at high temperatures induced by electron–phonon scattering.

References

1. D.R. Larson, W.R. Zipfel, R.M. Williams, S.W. Clark, M.P. Bruchez, F.W. Wise, W.W. Webb, Science **300**, 1434 (2003)
2. V. Sukhovatkin, S. Hinds, L. Brzozowski, E.H. Sargent, Science **324**, 1542 (2009)
3. M. Chamarro, F. Bernardot, C. Testelin, J. Phys. Condens. Matter. **19**, 44 (2007)
4. S. Fafard, R. Leon, D. Leonard, J.L. Merz, P.M. Petroff, Phys. Rev. B **50**, 11 (1994)
5. Maxim S. Gaponenko, Andrey A. Lutich, Nikolai A. Tolstik, Alexei A. Onushchenko, Alexander M. Malyarevich, Eugene P. Petrov, Konstantin V. Yumashev, Phys. Rev. B. **82**, 125320 (2010)
6. C. de Mello Donega, M. Bode, A. Meijerink, Phys. Rev. B **74**, 085320 (2006)
7. L. Zhang, T.A. Hill, C.H. Teng, B. Demory, P.C. Ku, H. Deng, Phys. Rev. B **90**, 245311 (2014)
8. S. Fafard, K. Hinzer, S. Raymond, M. Dion, J. McCaffery, Y. Feng, S. Charbonneau, Science **274**, 1350 (1996)
9. S. Fafard, R. Len, D. Leonard, J.L. Merz, P.M. Petroff, Phys. Rev. B **52**, 5752 (1995)
10. H. Klitabayashi, T. Wakoo, J. Cryst. Growth **150**, 152 (1995)
11. G.S. Solomon, J.A. Trezza, J.S. Harris, J. Appl. Phys. Lett. **66**, 3161 (1995)
12. T. Watanuki, S. Adachi, H. Sasakura, S. Mutoa, Appl. Phys. Lett. **86**, 063114 (2005)
13. AB Daly, MA Maaref, F. Bernardot, T. Barisien, C. Testelin, E. Galopin, A. Lemaitre, Solar energy and building (ICSoEB), IEEE (2015), pp. 1–4
14. T. Muller, F.F. Schrey, G. Strasser, K. Unterrainer, Appl. Phys. Lett. **83**, 17 (2003)
15. V.V. Belykh, A. Greilich, D.R. Yakovlev, M. Yacob, J.P. Reithmaier, M. Benyoucef, M. Bayer, Phys. Rev. B **92**, 165307 (2015)
16. A. Sahli, A. Melliti, M.A. Maaref, C. Testelin, A. Lemaître, R. Kuszelewicz, P. Voisin, Phys. Status Solidi (b) **244**, 2622 (2007)
17. M. Paillard, X. Marie, P. Renucci, J.-M. Amand, A. Jbeli, M. Gérard, Phys. Rev. Lett. **86**, 1634 (2001)
18. D. Bimberg, *Semiconductor Nanostructures* (Springer, Berlin, 2008)
19. R. Passler, J. Appl. Phys. **88**, 2570 (2000). **and references therein**
20. L. Vina, S. Logothetidis, M. Cardona, Phys. Rev. B **30**, 1979–1991 (1984)
21. R. Carles, N. Saint-Cricq, J.B. Renucci, M.A. Renucci, A. Zwick, Phys. Rev. B. **22**, 4804 (1980)
22. R. Carles, N. Saint-Cricq, J.B. Renucci, M.A. Renucci, A. Zwick, Solid State Commun. **59**, 869 (1986)
23. R. Passler, J. Appl. Phys. **89**, 6235 (2001)
24. G. Ortner, M. Schwab, M. Bayer, R. Passler, S. Fafard, Z. Wasilewski, P. Hawrylak, A. Forchel, Phys. Rev. B. **72**, 085328 (2005)
25. Z.Y. Xu, Z.D. Lu, X.P. Yang, Z.L. Yuan, B.Z. Zheng, J.Z. Xu, W.K. Ge, Y. Wang, J. Wang, L.L. Chang, Phys. Rev. B. **54**, 16 (1996)